Chelation of Serine 39 to Mg^{2+} Latches a Gate at the Active Site of Enolase: Structure of the Bis(Mg^{2+}) Complex of Yeast Enolase and the Intermediate Analog Phosphonoacetohydroxamate at 2.1-Å Resolution†,‡

Joseph E. Wedekind, Russell R. Poyner, George H. Reed,* and Ivan Rayment*

Institute for Enzyme Research, Graduate School, and Department of Biochemistry, College of Agricultural and Life Sciences, University of Wisconsin—Madison, Madison, Wisconsin 53705

Received March 14, 1994; Revised Manuscript Received May 24, 1994®

ABSTRACT: The structure of a new crystal form of enolase from bakers' yeast has been solved to 2.1-Å resolution. Crystals were grown from poly(ethylene glycol) and KCl at pH 8.2 in the presence of Mg^{2+} and a reaction intermediate analog, phosphonoacetohydroxamate (PhAH). Crystals belong to space group *C*2; have unit cell dimensions a = 123.5 Å, b = 73.9 Å, and c = 94.8 Å with β = 93.3°; and contain one dimer per asymmetric unit. The structure was solved by molecular replacement from the X-ray coordinates of apoenolase [Stec, B., & Lebioda, L. (1990) *J. Mol. Biol. 211*, 235–248]. Both essential divalent metal ions are observed to be complexed with the inhibitor. The two Mg^{2+} ions are 4.05 Å apart and are bridged by a μ-oxyl ligand from the carbonyl moiety of PhAH. The "high-affinity" Mg^{2+} coordinates to the carboxylate side chains of Asp 246, Glu 295, and Asp 320, one water molecule, and the hydroxamate and carbonyl oxygens of PhAH. The second Mg^{2+} coordinates to a phosphonyl oxygen, two water molecules, and the μ-bridge carbonyl oxygen of PhAH. Coordination schemes with respect to PhAH and water ligands are fully consistent with those of the Mn^{2+} complexes determined spectroscopically [Poyner, R. R., & Reed, G. H. (1992) *Biochemistry 31*, 7166–7173]. Remaining ligands for the second Mg^{2+} are the carbonyl oxygen and γ-oxygen of Ser 39. Chelation of this Ser residue to Mg^{2+} effectively "latches" a flexible loop extending from Gly 37 through His 43 and closes off the entrance to the active site. The position of the second Mg^{2+} in the active site provides new insight into the stereochemistry of substrate binding.

Enolase catalyzes the reversible dehydration of 2-PGA[1] to form P-enolpyruvate in the glycolytic pathway. The reaction is believed to proceed in a stepwise manner through a carbanionic intermediate at C2 of the substrate (Dinovo & Boyer, 1971; Stubbe & Abeles, 1980; Anderson & Cleland, 1990). The pK_a of the proton at C2 is high (~28–32); therefore, catalysis must include means for promoting rapid ionization of the carbon acid (Gerlt & Gassman, 1992), for stabilization of the *aci*-carboxylate form of the carbanion intermediate (Anderson et al., 1984), and for augmenting the leaving ability of OH^-. Similar carbanionic intermediates adjacent to carboxylate or carbonyl functions are most likely involved in the catalytic cycles of various other enzymes which catalyze eliminations or racemizations (Richard, 1990). Recent mechanistic proposals for promoting rapid ionization of the carbon acids to carbanions (Gerlt et al., 1991; Gerlt & Gassman, 1992) and for stabilization of these reactive species (Gerlt & Gassman, 1993) have renewed interest in this mechanistic problem.

Anderson et al. (1984) described a group of very tight binding inhibitors of enolase that mimic the structure of the proposed *aci*-carboxylate intermediate (**1**). One member of this group, PhAH (**2**), is the most potent inhibitor of enolase yet reported. The ionized form (pK_a 10.2) of this hydroxamic acid has a K_i of 15 pM.

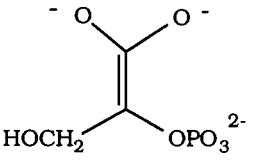

1

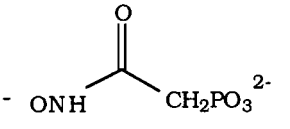

2

EPR spectroscopy has been used to investigate interactions of PhAH with the two metal ions at the active site of enolase (Poyner & Reed, 1992). In the bis(Mn^{2+}) complexes of the enzyme with PhAH, a strong electron spin exchange coupling between the Mn^{2+} centers indicated a close spacing of the Mn^{2+} ions. EPR measurements with ^{17}O-labeled forms of PhAH were used to determine points of coordination of the inhibitor with each metal ion. These experiments showed that the inhibitor binds to both metal ions in a binuclear chelate, **3**.

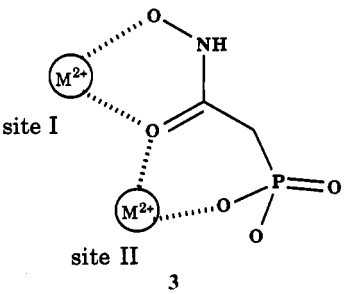

3

† This research was supported in part by NIH Grants GM35752 (G.H.R.) and AR35186 (I.R.) and by an NRSA Fellowship (J.E.W.) from NIH Training Grant GM08293.

‡ X-ray coordinates for this complex of enolase have been deposited in the Brookhaven Protein Data Bank under file name 1EBG.

* Address correspondence to these authors at the Institute for Enzyme Research, University of Wisconsin, 1710 University Ave., Madison, WI 53705.

® Abstract published in *Advance ACS Abstracts,* July 15, 1994.

[1] Abbreviations: 2-PGA, 2-phospho-D-glycerate; P-enolpyruvate, phosphoenolpyruvate; PhAH, phosphonoacetohydroxamate; PEG, poly(ethylene glycol); HEPES, 4-(2-hydroxyethyl)-1-piperazineethanesulfonic acid; EPR, electron paramagnetic resonance; rms, root mean square; PMSF, phenylmethanesulfonyl fluoride; HEPPS, 4-(2-hydroxyethyl)-1-piperazinepropanesulfonic acid; MES, 2-(*N*-morpholino)ethanesulfonic acid.

0006-2960/94/0433-9333$04.50/0

The μ-bridging carbonyl oxygen accounts for the strong electron spin exchange coupling in the bis(Mn^{2+}) complex. The favorable chelate rings provide a rationale for the high affinity of the inhibitor and suggest a possible role for both metal ions in stabilizing the enolate intermediate.

Several high-resolution structures of enolase have been reported by Lebioda and co-workers (Lebioda & Stec, 1989, 1991; Lebioda et al., 1989, 1993; Stec & Lebioda, 1990). These crystallographic studies have revealed much about the enzyme, including the overall tertiary fold of the protein, the binding site and protein ligands of metal I,[2] a direct interaction of metal I with 2-PGA, the position of the "phosphate" binding site, and a congregation of polar residues within the active site. The structure of the enolase–substrate[3] complex was used as a basis for discussion of a possible mechanism (Lebioda & Stec, 1991). However, the high concentration of $(NH_4)_2SO_4$ employed in the medium surrounding the crystals (Lebioda & Brewer, 1984; Lebioda & Stec, 1991) was not conducive to binding of the second equivalent of divalent cation.

Interest in contributions of the protein to the exceptional stability of the complex of PhAH with enolase and in the position of metal II in the active site prompted attempts at crystallization of the enolase–$(Mg^{2+})_2$–PhAH complex. PhAH is a slow-binding inhibitor (Anderson et al., 1984), and efforts were therefore focused on crystallization of the equilibrated enzyme–inhibitor complex. The present paper reports the high-resolution structure of the $(Mg^{2+})_2$–PhAH complex of the enzyme derived from crystals grown in solutions containing PEG at pH 8.2.

EXPERIMENTAL PROCEDURES

Protein Purification. Two procedures were used to purify yeast enolase for crystallization. Enzyme prepared by each method behaved similarly in crystallization experiments and migrated identically on SDS–PAGE and native PAGE gels. Early experiments used enzyme purified from moist bakers' yeast by the method described by Westhead (1966), as modified by Poyner and Reed (1992). Later experiments used enolase isolated from active dry bakers' yeast by a modification of the procedure reported by Lee and Nowak (1992). Centrifugation and $(NH_4)_2SO_4$ fractionation were carried out at 4 °C, while most other steps were performed at room temperature. In a typical preparation, 2 lb of Red Star instant active yeast was lysed by stirring overnight (12–14 h) in 2 L of 0.5 N NH_3(aq) containing 5 mM EDTA (Scopes, 1971). Next, 1 L of 1 M acetic acid was gradually added, followed by 0.7 g of PMSF dissolved in 50 mL of absolute ethanol. The suspension was then adjusted to pH 7 with 1 M Tris base. Cell debris was removed by centrifugation at 5000*g* for 30 min. The supernatant was then fractionated by $(NH_4)_2SO_4$ precipitation as described by Lee and Nowak (1992). The final $(NH_4)_2SO_4$ pellet was resuspended in 800 mL of 1 mM $Mg(OAc)_2$ and 0.1 mM EDTA/Tris, pH 8, and desalted on a 10 × 60 cm column of coarse Sephadex G-50 equilibrated with the resuspension buffer. 1 M Tris/HCl, pH 8.0, was added to the desalted enzyme to a final concentration of 20 mM. The protein solution was filtered through a 6 × 13 cm cake of coarse, fibrous DEAE-cellulose (equilibrated with 20 mM Tris/HCl, pH 8.0) in a Büchner funnel. The cellulose was washed with 1 L of 20 mM Tris/HCl, pH 8.0, and the washes were combined with the clear filtrate. The combined solution was adjusted to pH 5.9 with solid MES and applied to a 5 × 20 cm column of CM Sephadex C-50 equilibrated with 20 mM MES and 0.2 mM EDTA, pH 6.0 (buffer A). The column was washed with 1 L of buffer A and eluted with a 2-L linear gradient from 0 to 0.25 M KCl in buffer A. Enolase activity eluted in a single peak between 125 and 175 mM KCl. Fractions containing enolase were pooled, concentrated by precipitation with 80% saturated $(NH_4)_2SO_4$, and dialyzed at 4 °C against 20 mM Tris/HOAc, pH 8.0, containing 2 mM $Mg(OAc)_2$, 0.2 mM EDTA, and 0.02% (w/v) NaN_3. The enzyme was concentrated to approximately 55 mg mL^{-1} in an Amicon ultrafiltration pressure cell at room temperature. Protein solutions were stored on ice or at 4 °C prior to crystallization. All dilutions of the protein were made with the dialysis buffer.

Materials. PhAH was synthesized according to the procedure of Anderson et al. (1984) as modified by Poyner and Reed (1992).

Screening of Crystallization Conditions. A series of crystallization trials was carried out at 20 °C by the vapor diffusion method in the presence and absence of the inhibitor. PEG 3350 and 8000 were tested between 12 and 28% (w/w) in combination with 0.2–0.5 M sulfate salts of Mg^{2+}, Li^+, Na^+, NH_4^+, and K^+; the Na^+ and K^+ salts of phosphate; and the Cl^- salts of $N(CH_3)_4^+$, NH_4^+, Na^+, and K^+. A range of pHs between 7.0 and 8.5 was included. Protein concentrations were between 10 and 28 mg mL^{-1} in droplets prior to equilibration.

Crystal Growth. Small single crystals of inhibitor-free enzyme resulted from trials in which 20 mg mL^{-1} protein was equilibrated by vapor diffusion against 20–28% PEG 8000, 0.3 M KCl, and 25 mM HEPES/NaOH, pH 7.0. Larger crystals of inhibitor-free enzyme were grown by batch through a microseeding (McPherson, 1982) process that utilized the initial crystals. Batch procedures were adopted because spontaneous nucleation of the original vapor diffusion experiments was irreproducible. The final batch crystallization procedure required the addition of equal volumes of protein and precipitant solution to give a final volume of 0.25–0.50 mL. The precipitant consisted of 32% (w/w) PEG 8000, 0.5 M KCl, and 80 mM HEPPS/NaOH, pH 8.0. This solution was added, dropwise, to the solution of concentrated protein with mild vortexing at room temperature. Approximately 30 μL was added every 10 s. The resulting slightly turbid mixture was transferred to an acid-washed and silanized Kimble shell vial (i.d. 6 or 8 mm, 0.25 or 0.5 dram) and sealed with a rubber septum. After approximately 24 h, the turbidity cleared. Microseeds were captured on a keratin bristle and applied in a single stroke to the walls of the shell vial. Crystals, approximately 1.0 × 0.5 × 0.5 mm, were obtained in 2 weeks. Crystals belonged to space group $P2_1$ and had unit cell dimensions of a = 72.5 Å, b = 73.2 Å, and c = 89.1 Å, with β = 104.4°. Crystals have one dimer per asymmetric unit and diffract to 1.8-Å resolution. These inhibitor-free crystals were used as microseeds for batch experiments in the presence of the inhibitor in an attempt to cross-seed the crystallization solutions using epitaxial nucleation (Thaller et al., 1985; McPherson & Shlichta, 1988). Successful cocrystallization resulted when a solution of 33.5–34% (w/w) PEG 8000, 0.5 M KCl, and 80 mM HEPPS/NaOH, pH 8.0, was mixed, as

[2] In much of the previous literature on enolase, the metal ion which binds tightly to enolase in the absence of substrates has been called the "conformational" metal. The second metal ion which binds to enolase in the presence of substrate has been called the "catalytic" metal ion. We will refer to the two divalent cations in order of decreasing binding affinity as metal I and metal II, respectively.

[3] The term "substrate" is used to denote a mixture of 2-PGA and P-enolpyruvate that was present in the crystals studied by Lebioda and Stec (1991). Under physiological conditions the internal equilibrium constant of enolase is approximately unity (Burbaum & Knowles, 1989).

Table 1: Intensity Statistics for the Native X-ray Data Set

		shell (Å)									
	total	100–6.63	–4.69	–3.83	–3.32	–2.97	–2.71	–2.51	–2.35	–2.21	–2.10
observations	84862	4024	10947	13053	13750	13652	11907	6133	4507	4084	2805
total independent	38673	1591	2935	3755	4434	4963	5248	4564	4337	4047	2799
reflections[a]		(1000)	(2483)	(3149)	(3551)	(3715)	(3313)	(1062)	(170)	(37)	(6)
theoretical (%)	77	96	100	100	100	99	94	76	68	56	40
intensity (av)		816	702	966	614	376	259	181	154	163	118
σ		30	32	43	34	29	26	24	24	27	28
R-factor[b] (%)	4.7	2.3	3.0	3.0	3.9	5.5	7.1	9.5	10.7	11.3	16.6

[a] This is the number of reduced observations. Shown in parentheses is the number of independent measurements for which there were duplicate or symmetry-related observations. [b] R-factor = $(\Sigma|I - \bar{I}|/\Sigma I) \times 100$.

described for the inhibitor-free experiments, with an equal volume of 33 mg mL^{-1} enolase containing 4 mM $MgCl_2$ and 4 mM PhAH. The pH after equilibration was 8.2. The opaque protein precipitant mixture was transferred to a Plexiglas depression plate capable of holding ~0.5 mL and microseeded immediately. Prior to use, the wells of the depression plate were coated with a thin layer of Dow Corning silicone grease 4. Plates were sealed with glass cover slips and vacuum grease. Crystals were 0.3 × 0.5 × 1.8 mm in size and diffracted beyond 2.0-Å resolution. Data were recorded to 2.1-Å resolution in the present study. Crystals had the following properties: space group $C2$; unit cell dimensions a = 123.5 Å, b = 73.9 Å, and c = 94.8 Å, with β = 93.3°; one dimer per asymmetric unit.

X-ray Data Collection and Processing. Crystals were mounted in quartz capillary tubes (Rayment, 1985) and characterized by precession photography. Photographs were recorded for 18 h with a crystal-to-film distance of 10 cm. X-ray intensities were collected at 4 °C on a Siemens X-1000D multiwire area detector at a crystal-to-detector distance of 17 cm using Ni-filtered Cu Kα radiation from a Rigaku RU 200 rotating anode X-ray generator with a 200-μm focal spot, operated at 50 kV × 50 mA. Diffraction data from three crystals were processed with the XDS data reduction software of Kabsch (1988a,b) and scaled by the method of Fox and Holmes (1966), giving a data set that was 77% complete to 2.1-Å resolution. The overall merging R-factor for the intensity data was 4.7% (Table 1).

Molecular Replacement. The molecular structure of the enolase–$(Mg^{2+})_2$–PhAH complex was solved by molecular replacement with the AMORE software programs of Navaza (1987, 1990) starting from the coordinates of an apoenolase described by Stec and Lebioda (1990). A single subunit was used as the search model. An initial cross-rotation function, calculated from X-ray data between 4.0- and 8-Å resolution, generated two sets of peaks of approximately equal height. Members of each set were related by 180°. A single solution was chosen having Euler angles α = 173.3°, β = 106.5°, and γ = 323.5°. The location of one subunit was determined by the corresponding translation function and gave a translational component of a = 0.125, b = 0.358, and c = 0.692. Upon fixation of this solution, other rotation function solutions were applied to the search model, and the translation function was solved in order to reveal the position of the second subunit. Solutions were examined on a graphics system using the program FRODO (Jones, 1978), and the correct noncrystallographic dimer was chosen. Fast rigid body refinement (Castellano et al., 1992) improved the solutions and resulted in an initial crystallographic R-factor of 43.6% for all measured data to 2.7-Å resolution.

Electron Density Modification. Crystallographic least-squares refinement of the preliminary model by the program TNT (Tronrud et al., 1987) reduced the R-factor to 36% for all data to 2.7-Å resolution. Model phases were improved by cyclical molecular averaging of the two subunits in the asymmetric unit (Bricogne, 1976). The refined dimer coordinates were used to derive a rotation matrix and to define a molecular envelope for a single subunit at 5.0-Å resolution.

The electron density map for the first cycle of refinement was calculated from reduced-bias coefficients $(2m|F_o| - D|F_c|)$ in order to suppress the model bias, where the weights (m and D) were derived from the SIGMA A scheme (Read, 1986). F_o represents the experimentally observed structure factor amplitudes, and F_c represents those calculated from the refined model. Initially the phase refinement was performed at 2.7-Å resolution for 15 cycles.

The enolase chain was manually rebuilt into the phase-refined and averaged electron density map for one subunit using the program FRODO. Thereafter the subunit was returned to the unit cell and further refined by crystallographic least squares for 12–16 cycles. This process of phase refinement, model building, and crystallographic refinement was repeated two more times, first at 2.7- and then at 2.1-Å resolution. During the second round of rebuilding, Mg^{2+} I and a phosphate were introduced, although both Mg^{2+} ions and the inhibitor were visible. After phase refinement at 2.1-Å resolution, PhAH, Mg^{2+} II, and approximately 60 waters were added to the model. In addition Gly 37, Gly 41, and Val 42 were fitted into the density. These residues were removed previously from the model because they had no electron density beyond the noise level in the initial averaged map. PhAH was modeled by version 2.5 of the Macromodel computer graphics program (Still, 1989). Bond distances and geometries for the phosphonate portion of the inhibitor were obtained from small molecule crystal structures. Representative structures are those of Bowen et al. (1982) and Zanotti et al. (1984). Details of the hydroxamate portion of PhAH were derived from the siderophore crystal structures of Zalkin et al. (1966) and Hough and Rogers (1974). Upon completion of rebuilding the subunit into averaged density at 2.1-Å resolution, the molecule was placed back into the crystallographic cell and refined by least squares for eight cycles. Coefficients of the form $(2F_o - F_c)$ and $(F_o - F_c)$ were used to calculate unaveraged maps for the molecular dimer. Initial fitting revealed the positions of six previously missing amino acids, Ala 38, Ser 39, and Thr 40, which now exhibited well-defined features for side chains and carbonyl oxygens, in each respective subunit. Presently, 356 water molecules (temperature factors ≤ 66 $Å^2$) have been included in the dimeric model.

The final crystallographic R-factor was 18.6% for all measured data to 2.10-Å resolution. The rms deviations from ideal geometry are 0.015 Å for bond lengths, 2.1° for bond angles, and ≤0.008 Å for coplanar groups. A Ramachandran

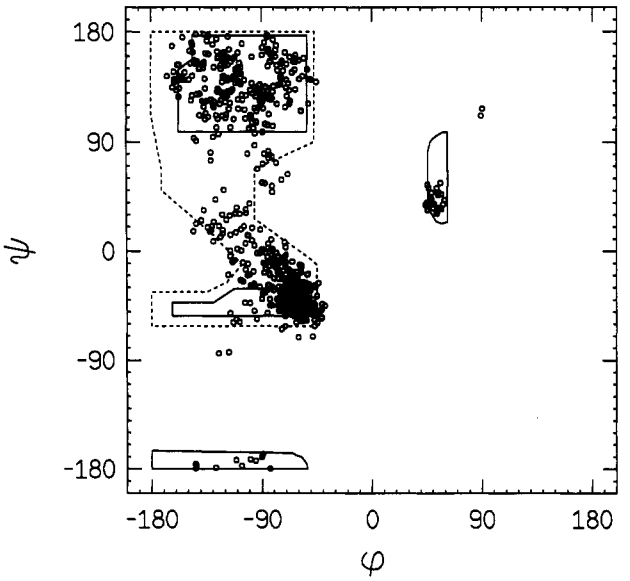

FIGURE 1: Ramachandran plot of dimeric yeast enolase main-chain non-glycinyl dihedral angles. Fully allowed φ and ψ values are shown by solid enclosures. Partially allowed regions are enclosed by broken lines. Dihedral angles for the most severe outliers are distorted by hydrogen bonding. In both subunits, the left-handed helical outlier is Arg 402 whose guanidinium group strongly interacts with Glu 404. Other outliers from both subunits include metal ligands Asp 320 (−120, −80) and Ser 39 (−89, 67).

plot for the dimer main-chain non-glycinyl dihedral angles is given in Figure 1.

RESULTS AND DISCUSSION

Electron Density. Figure 2 shows representative electron density calculated from the coefficients $(2F_o - F_c)$. All residues have well-defined carbonyl oxygens and side chains except those listed in Table 2. All disordered residues lie on the protein surface exposed to solvent. In previous structures residue 84 was modeled as a Ser (Lebioda et al., 1989) consistent with amino acid sequencing of the protein (Chin et al., 1981). Density observed in the present map is consistent with a Lys (Figure 2b) consistent with the nucleotide sequence of Holland et al. (1981).

Electron density extending from Asn 266 through Lys 269 is weak in both subunits. These four residues are located in a flexible loop at the surface of the protein. However, Pro 265 at the beginning of this region is clearly in the *trans* configuration. Previous crystal structures modeled Pro 265 in the *cis* conformation. This isomerization has no impact on the topology of the polypeptide chain but creates a tight turn that allows formation of a hydrogen bond between the carbonyl oxygen of Asn 264 and the amide hydrogen of Ser 267.

Polypeptide Fold. The chain topology of the enolase–PhAH complex described here is identical to that observed previously (Lebioda et al., 1989). Subunits of enolase have two domains. The N-terminal domain extends over residues 1–142 and consists of a three-stranded antiparallel β-meander followed by four α-helices. The C-terminal domain is an eight-stranded mixed α/β-barrel with the connectivity $\beta\beta\alpha\alpha(\beta\alpha)_6$ (Stec &

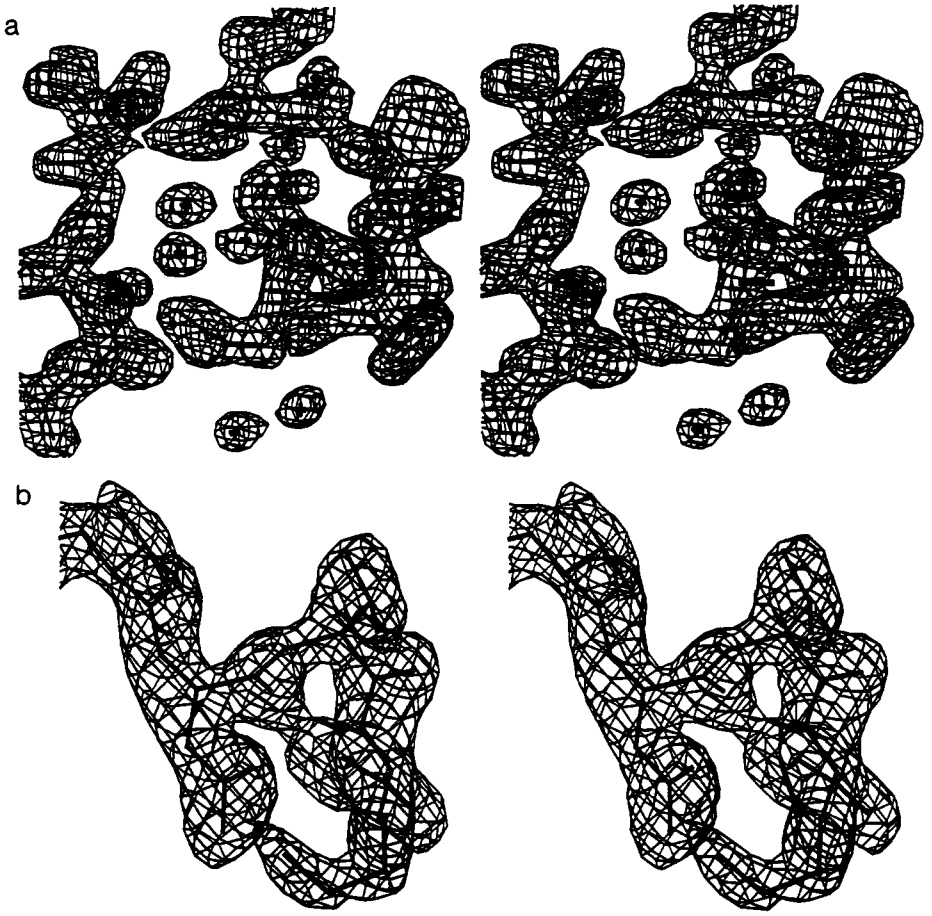

FIGURE 2: Representative portions of $(2F_o - F_c)$ electron density maps calculated with the final refined phases. (a) Electron density contoured at 1σ for residues 36–42 of the active site loop (left) and residues 249–253 and 299–300 of the subunit I C-terminal domain. (Residue 250 was omitted for clarity). The waters shown participate in closure of the active site through hydrogen bonding. (b) Electron density contoured at 1.25σ for Ile 81, Asp 82, Val 83, and Lys 84 on the surface of subunit I. This figure and Figure 5 were generated by FROST (G. Wesenberg, University of Wisconsin).

Table 2: Disordered Side Chains[a]

amino acid subunit I	disordered atoms	amino acid subunit II	disordered atoms
Lys 27	ε, ζ	Lys 27	ε, ζ
Lys 53	δ, ε, ζ	(Gln 277)[b]	(O, water)
Lys 59	δ, ε, ζ	Lys 59	ε, ζ
Lys 78	γ, δ, ε	Lys 78	δ, ε, ζ
(Ala 79)[b]	(O, water)	Asn 80	Cγ, Oδ1, Nδ2
Lys 87	ε, ζ	Lys 87	δ, ε, ζ
Lys 104	δ, ζ	Lys 104	ε, ζ
Lys 138	δ, ε, ζ	Lys 138	ε, ζ
		Lys 140	δ, ε, ζ
Lys 177	δ, ε, ζ	Lys 177	γ, δ, ε, ζ
		Lys 199	γ, δ, ε, ζ
Asp 238	Oδ1, Oδ2	Asp 238	Oδ1, Oδ2
Asp 255	Cγ, Oδ1, Oδ2	Asp 255	Cγ, Oδ1, Oδ2
Lys 257	ε, ζ	Lys 257	δ, ε, ζ
Asn 266	Cγ, Oδ1, Nδ2	Asn 266	Cγ, Oδ1, Nδ2
Asp 268	Oδ1, Oδ2	(Ser 142)[b]	(Oγ)
Lys 269	ε, ζ	Lys 269	δ, ε, ζ
Lys 271	ε, ζ	Lys 271	ε, ζ
Glu 304	Cδ, Oε1, Oε2	Glu 304	Cδ, Oε1, Oε2
(His 308)[b]	(Nε2)	Lys 311	δ, ε, ζ
Lys 328	ε, ζ	Lys 328	δ, ε, ζ
(Asp 101 & Ser 103)[b]	(Nδ2 & Oγ)	Glu 335	Cδ, Oε1, Oε2
Lys 337	δ, ε, ζ	Lys 337	δ, ε
		Asp 421	Cγ, Oδ1, Oδ2
		Glu 428	Cδ, Oε1, Oε2
		Lys 435	δ, ε

[a] Atoms have negligible electron density > 1.0σ and $B \geq 95$ Å^2. [b] Atoms of residues in parentheses provide crystal contacts that eliminate disorder experienced by residues of the dyad-related subunit.

Lebioda, 1990). The active site is located at the carboxylic end of the barrel among loops contributed by both domains. The α-carbons of the independently modeled subunits superimpose with an rms deviation of 0.19 Å.

To determine which regions of the protein were influenced by the binding of PhAH and the second Mg^{2+}, the structure of the enolase–PhAH complex was superimposed on the structure of apoenolase (Stec & Lebioda, 1990) and on the structure of substrate-bound enolase (Lebioda & Stec, 1991) by the algorithm of Kabsch (1978). Figure 3 shows a comparison of apoenolase and enolase–$(Mg^{2+})_2$–PhAH structures. The N-terminal domains of the two structures align with an rms deviation of 0.34 Å, provided residues 37–43 (the active site loop) are excluded. Inclusion of the active site loop increases the rms deviation to 1.56 Å. Equivalent comparisons of the enolase–$(Mg^{2+})_2$–PhAH structure and the substrate-bound enolase (Lebioda & Stec, 1991) result in rms deviations of 0.35 and 0.63 Å, respectively. The orientation of the N-terminal domains relative to the dimer dyad is very similar for all three enolase structures, and this domain provides a reference for the more substantial movements that occur in the C-terminal domains (Figure 3a). When PhAH and the second divalent cation bind to the enzyme, the active site cleft closes. The rms deviation of the C-terminal domain in the PhAH enzyme complex from that of the apoenzyme is 1.37 Å. Figure 3b illustrates the movement of two particular C-terminal segments comprising residues 155–165 and 251–284. Removal of these residues from the "apo" versus the "PhAH" superposition lowers the rms deviation to 0.77 Å. Analogous superpositions of the C-terminal domains of the PhAH and substrate-bound enolase structures give rms deviations of 1.14 and 0.57 Å. The latter comparison indicates that when the substrate binds to the enzyme in a high-salt, low-pH environment without the second divalent cation, the active site closes, but not to the extent observed in the enolase–$(Mg^{2+})_2$–PhAH complex. The superposition analysis indicates that binding of PhAH and Mg^{2+} II is accompanied by a series of new interactions concentrated at the active site but propagated to more remote regions throughout the structure.

Temperature Factors. Temperature factors were restrained between 1 and 100 Å^2 during the refinement. The average temperature factors for all atoms in subunits I and II were 23.4 and 27.9 Å^2, respectively. Differences in temperature factors between the two subunits most likely arise from the packing arrangement of the subunits in the crystal lattice.

Comparison of the temperature factors of various enolase structures reveals three regions where differences are localized (Figure 4). These regions exhibit lower temperature factors in the enolase–Mg^{2+}–PhAH complex than those of the apo and substrate-bound forms of enolase. Reduction in temperature factors in the PhAH complex correlates with the direct interaction of mobile elements to the inhibitor or metal II.

Active Site. The fit of the inhibitor and metals to the electron density is unambiguous (Figure 5a). The validity of the fit was demonstrated by re-refining the structure in the absence of Mg^{2+} II, its water ligands, and the inhibitor and then computing difference electron density maps (Figure 5b). The phosphonate moiety of PhAH is exceptionally well defined in these difference maps as indicated by the tri-lobed nature of the electron density encompassing the phosphonyl oxygens. The asymmetric fit of the inhibitor into the electron density precludes other chemically reasonable alternative conformations of the molecule.

Mobile Elements. In the PhAH complex, the phosphonyl oxygens make hydrogen bond contacts with the amide hydrogens of Ala 38, Ser 39, and Ser 375 as well as the side chains of Arg 374, Ser 375, and His 159. These contacts (except for Ser 375 and Ser 39) appear in the enolase–Mg^{2+}–F–P_i complex (Lebioda et al., 1993). Interaction of Ser 39 and His 159 with PhAH anchors two flexible loops that effectively close off the active site in the enolase–PhAH complex (Figures 6 and 7). Residues 247–284 undergo the largest movement of any contiguous region of the chain. Of these residues, approximately half form a hydrophobic core which originates in the strand 3/helix C loop (residues 247–274) and extends through the barrel-exposed side of helix C (275–288; see Figure 3b). Movement of His 159 toward PhAH generates a cavity adjacent to this peripheral hydrophobic pocket. Reorientation of the ε-amino group of Lys 263 into this cavity establishes hydrogen bonds to the carbonyl oxygens of Ala 160, Gly 162, and Leu 164 of the His 159 loop. Because Lys 263 is tethered to the hydrophobic core, this latter region must adjust to maintain the van der Waals contacts of the core interior. Other contacts at the active site are shown in Figure 2a. Water-mediated hydrogen bonds link the carboxylic groups of Glu 251 and Glu 300 to the carbonyl oxygen of Thr 40. In addition, the side chains of Ser 250 and Glu 300 hydrogen bond directly to the amide hydrogens of Glu 300 and Val 42, respectively.

Metal Coordination. Figure 5a reveals well-defined electron density corresponding to both Mg^{2+} ions and their ligands. Each Mg^{2+} has octahedral coordination geometry, and both ions coordinate to the inhibitor. Lobes of electron density clearly define the waters in the coordination sphere of each Mg^{2+}. Consistent with previous structures (Lebioda & Stec, 1989), metal I coordinates to carboxylate oxygens from the

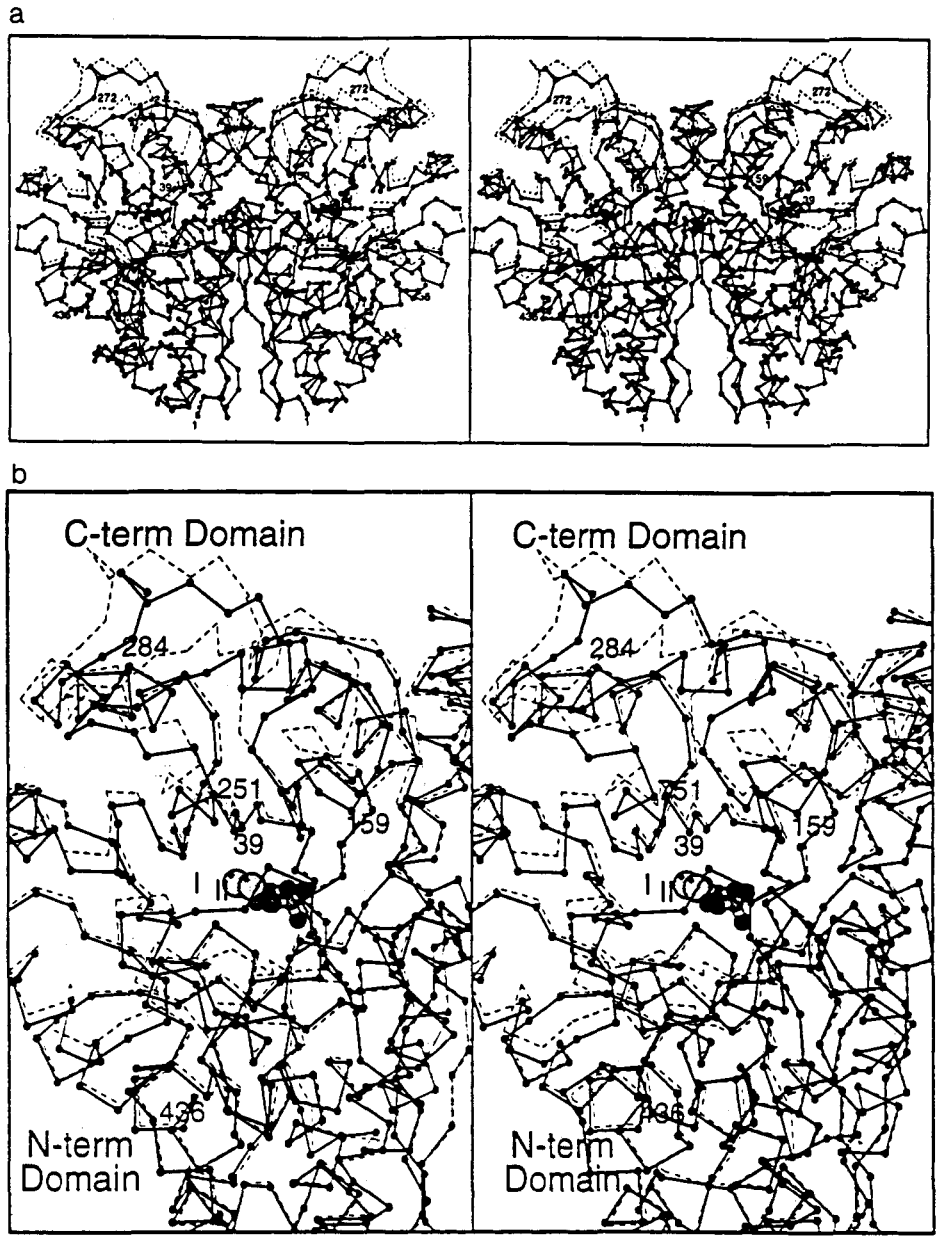

FIGURE 3: Superposition of the Cα coordinates of the enolase–$(Mg^{2+})_2$–PhAH complex and the "apo" enzyme. Solid lines represent the enolase–PhAH structure. The inhibitor and the metals are represented as ball-and-stick and space-filling models, respectively. Broken lines represent the apo structure. (a) Global view of the dimer, perpendicular to the noncrystallographic dyad. Subunit II is at left. (b) Close-up view of the C-terminal domain of subunit II. Metal ions are labeled I and II. The center of helix C is labeled 284. This figure and Figure 6 were generated by MOLSCRIPT (Kraulis, 1991).

side chains of Asp 246, Glu 295, and Asp 320. Other ligands of metal I are a water molecule and the hydroxamate oxygen of PhAH. The carbonyl oxygen of PhAH acts as a μ ligand between the metals (Figure 6). In addition, metal II coordinates a phosphonyl oxygen of PhAH, two water molecules, and the carbonyl oxygen and γ-oxygen of Ser 39. The oxygen–metal–oxygen angle formed by the Mg^{2+} I chelate is 75°. This distortion correlates with the larger zero field splitting anisotropy in the EPR spectrum of Mn^{2+} in this site. The active site loop, or gate, that encloses the inhibitor and Mg^{2+} II is hinged in part by Gly 37 and Gly 41, which allow Ser 39 to rotate into a position where its carbonyl oxygen and γ-oxygen coordinate Mg^{2+} II. Chelation of Ser 39 to Mg^{2+} II functions as a "latch" to secure this gate, effectively sealing off the active site (Figures 6 and 7). This intricate chelation mechanism for active site closure is one of the more intriguing observations to come from this crystal structure. Breaking of Thr 35 O^{γ}–Mg^{2+} coordination in the "GTP form" of *ras* p21 is a part of the "molecular switch" transition in this protein that accompanies hydrolysis of GTP (Milburn et al., 1990), although in this latter protein the carbonyl oxygen of Thr 35 is not coordinated to the Mg^{2+}.

The binuclear chelate structure of the enzyme-bound $(Mg^{2+})_2$–PhAH complex, as well as the hydration of metals I and II, agrees with the structure derived from the EPR measurements of Poyner and Reed (1992). In particular, the μ ligand contributed by PhAH brings the two metals to within 4.0 Å. The close spacing of the metal centers, together with superexchange mediated by the μ ligand, accounts for strong electron spin exchange coupling present in the analogous bis-(Mn^{2+}) complex. The favorable chelate rings established by coordination to the two metal ions undoubtedly contribute substantially to the tight binding of PhAH.

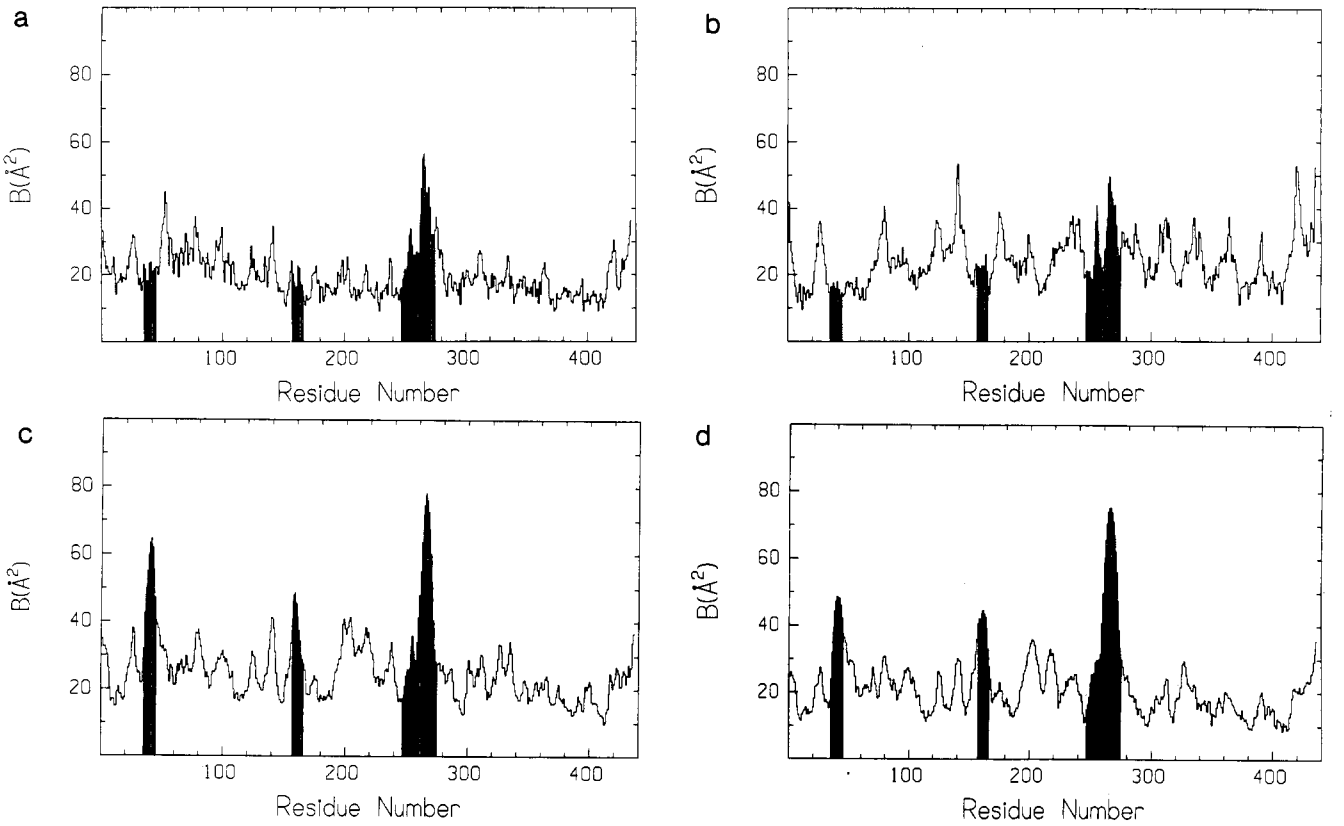

FIGURE 4: Mean temperature factor vs amino acid residue for all subunit main-chain atoms. Shaded areas denote structural regions in the PhAH-bound enzyme that have significantly moved compared to the apo and substrate-bound enolase structures. (a) Subunit I of the enolase–$(Mg^{2+})_2$–PhAH complex, (b) subunit II, (c) apoenolase, and (d) substrate-bound enolase. Temperature factors for the latter two plots were extracted from X-ray coordinates 3enl and 7enl, respectively (Stec & Lebioda, 1989; Lebioda & Stec, 1991), deposited in the Protein Data Bank (Bernstein et al., 1977).

Polar side chains line the active site (Figure 6). The side chains from His 373, Glu 211, and Glu 168 project toward one surface of the bound inhibitor, and the side chain of Lys 345 points toward the opposite surface of the inhibitor. N^{ζ} of Lys 396 is positioned to hydrogen bond to the hydroxamate oxygen. These residues are highly conserved[4] among enolase sequences. As shown in Figure 6, the positions of the side chains of these residues are virtually unchanged between the PhAH- and substrate-bound structures. This finding is somewhat surprising because the substrate structure was termed "precatalytic", and substantial movements of these side chains were necessarily invoked to accommodate their presumed catalytic functions (Lebioda & Stec, 1991). Yet, even with a tight-binding, intermediate analog and both divalent cations in place, the positions of these side chains remain essentially fixed, and interior regions of the active site are not altered.

A water molecule positioned between Glu 211 and Glu 168 in the model of the substrate complex has been posited as a candidate for the catalytic base (Lebioda & Stec, 1991). The catalytic activity of the E168Q mutant is suppressed by $\geq 10^4$, which is consistent with an important catalytic function for Glu 168 (Brewer et al., 1993). Additionally, an isotope effect on inhibition by D-tartronate semialdehyde 2-phosphate indicates that the catalytic base has a low $^2H/^1H$ fractionation factor (Weiss et al., 1987) suggestive of a functionality such as H_3O^+ as the conjugate acid (Cleland, 1992).

[4] Enolase sequences from 20 sources, including duck, contain Lys at positions equivalent to 345 and 396 of the yeast enzyme in highly conserved motifs, LLL[345]KVNQIGS(T) and TGQI[396]KTGAP, respectively. The chemically determined sequence analysis of enolase from chicken indicates Gly and Glu at positions 345 and 396, respectively (Russell et al., 1986).

Despite the apparent cohesion associated with the suggested model for the general base catalyst in enolase, the structural basis for the model is not without ambiguity. In particular, Lebioda and Stec (1991) noted that the orientation of the substrate with respect to rotation about the C2–OP bond was somewhat questionable, because the electron density did not permit a clear distinction between the positions of the carboxylate and hydroxymethyl groups of 2-PGA. The alternative orientation for the carboxylate and hydroxymethyl groups of 2-PGA brings the ionizable proton at C2 to the opposite side of the active site where it would encounter a more "conventional" base—the ϵ-amino group of Lys 345. A precedent for Lys acting as a general base in a related enzyme, mandelate racemace, is well established (Neidhart et al., 1991; Petsko et al., 1993; Landro et al., 1994).

PhAH versus 2-PGA. Although PhAH is the highest affinity inhibitor known for enolase, it is not isostructural with the presumed intermediate. The absence of a carboxylate group or a nitro analog thereof in PhAH cannot be dismissed. Nevertheless, the implications of the enolase–$(Mg^{2+})_2$–PhAH structure are worthy of exploration. The tight-binding behavior of PhAH was attributed to the structural similarity between PhAH, **2**, and the *aci*-carboxylate intermediate, **1**. The significance of an sp^2-hybridized carbon, the carbonyl carbon of PhAH and C2 of the putative intermediate, as well as the positions of the hydroxymethyl moiety of the intermediate and the hydroxyamino moiety of PhAH, was noted (Anderson et al., 1984). Choosing the rotamer of 2-PGA which places the hydroxymethyl and carboxylate moieties of 2-PGA in positions analogous to those of the hydroxyamino and carbonyl moieties of PhAH, respectively, projects the

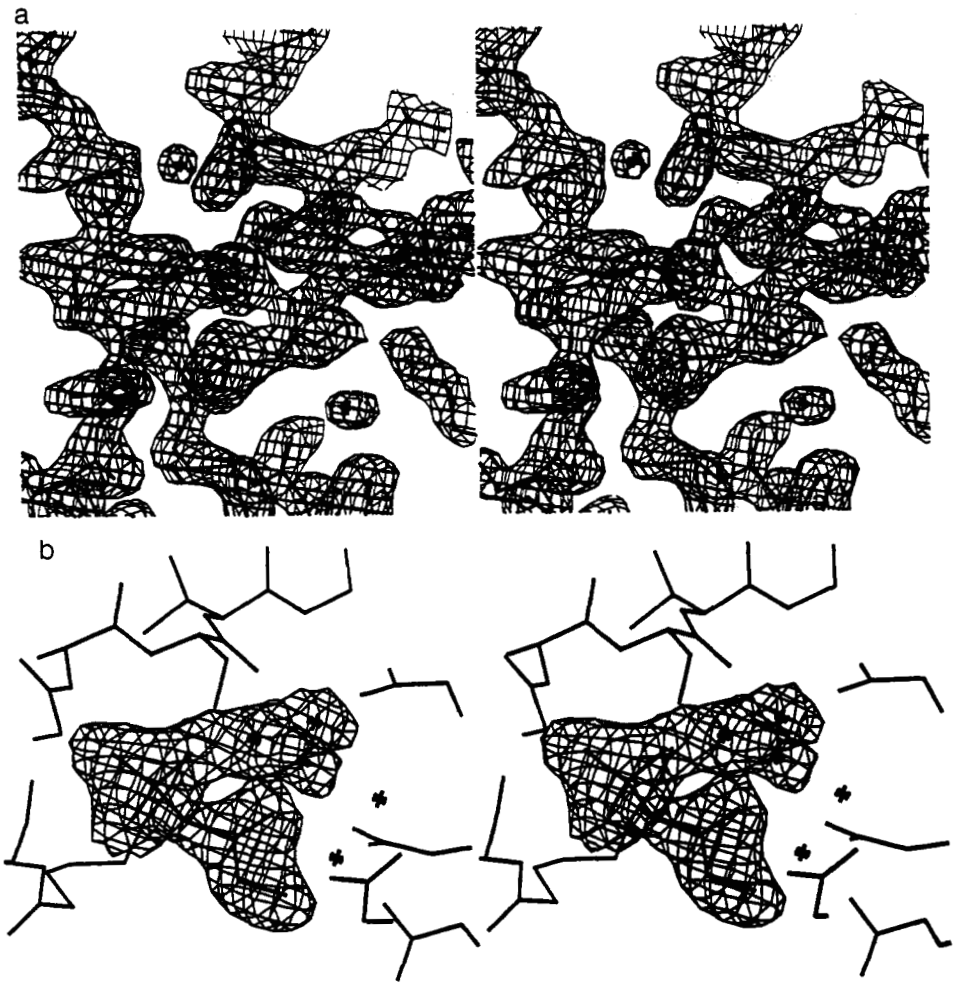

FIGURE 5: Electron density maps of the active site of the enolase–$(Mg^{2+})_2$–PhAH complex. (a) $(2F_o - F_c)$ electron density contoured at 1.5σ showing the interaction of metals I and II with their respective ligands including the inhibitor. The view is a cross section through the barrel of subunit II. (b) $(F_o - F_c)$ electron density contoured at 2.0σ for PhAH, Mg^{2+} II, and two waters. Ser 39 is directly above Mg^{2+} II. The view is from inside the barrel of subunit I.

ionizable proton at C2 toward Lys 345 and places the carboxylate group in a position bridging the two metals (**4**).

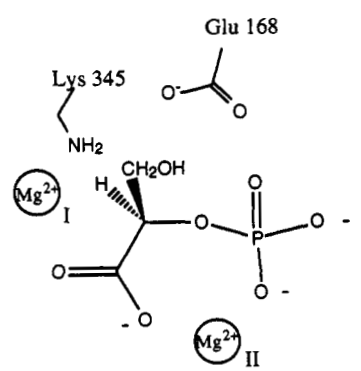

4

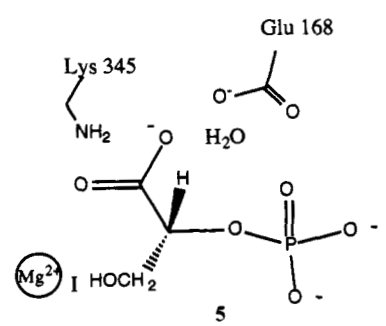

5

The mechanistic advantage of a bridging carboxylate group in stabilization of the *aci*-carboxylate intermediate has been discussed (Poyner & Reed, 1992). Metal II would be especially effective in this proposed function because its charge is attenuated by only one other anionic ligand.

Conversely, the rotamer of 2-PGA (**5**) corresponding to that described in the mechanism proposed by Lebioda and Stec (1991) places the hydroxymethyl moiety in the region occupied by the bridging carbonyl group of PhAH. A search of the Cambridge Structural Data Base for alcoholic bridging groups revealed no such examples with alkaline earth metal ions. In contrast, the database contains numerous examples of bridging carboxylate ligands for complexes of alkaline earth metal ions. The possibility that metal II binds in different positions in the inhibitor and substrate complexes appears to be unlikely given the facility with which the loop anchored by Ser 39 closes around metal II. Further structural evidence exists that the μ-carbonyl bridge in the PhAH complex is not accidental. Recent EPR measurements with Mn^{2+} and ^{17}O-labeled substrate show that metal II chelates to the phosphate and carboxylate groups of the substrate (R. R. Poyner and G. H. Reed, unpublished observations). Hence, the alternative stereochemistry of substrate binding (**4**) resembles the binding of PhAH and agrees with independent spectroscopic measurements. These new stereochemical considerations suggest that Lys 345 should not yet be ruled out as the general base catalyst. As demonstrated by the dramatic loss of catalytic

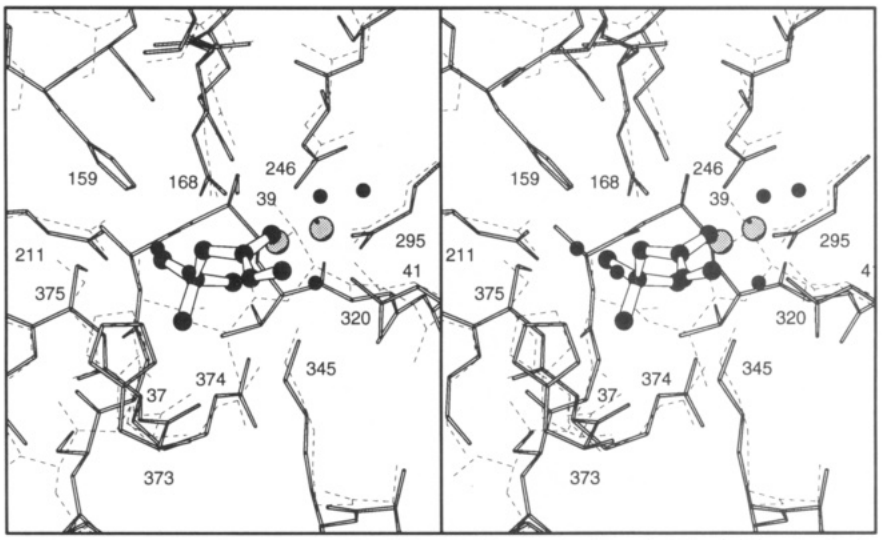

FIGURE 6: Close-up view of the active site of the enolase–$(Mg^{2+})_2$–PhAH complex from inside the barrel of subunit II. Amino acids are represented as sticks. Broken lines represent superimposed residues from the 2-PGA/P-enolpyruvate bound enzyme (Lebioda & Stec, 1991). PhAH and the metal ions are represented as ball-and-stick and space-filling models, respectively. Dark spheres represent waters.

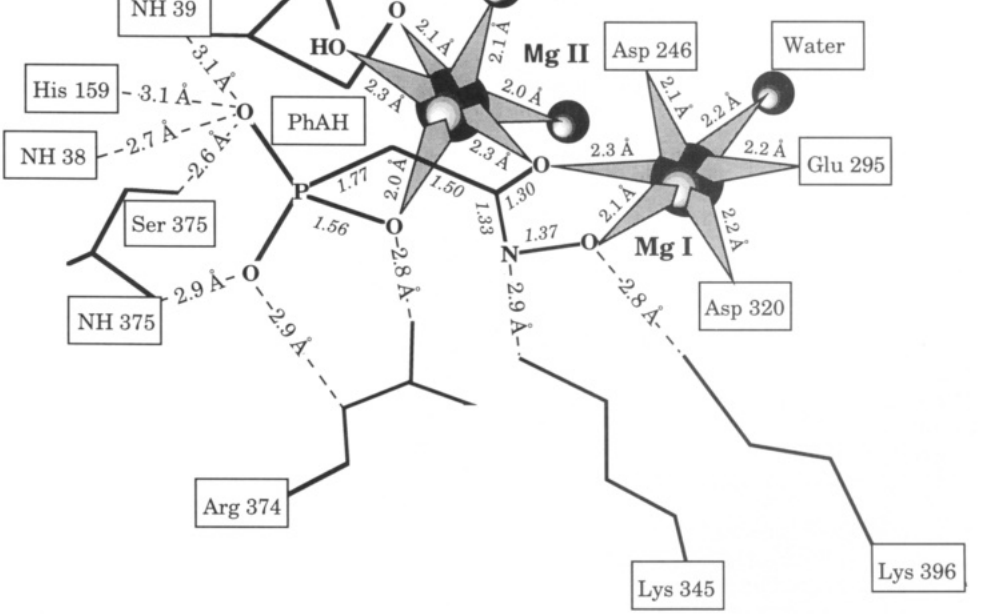

FIGURE 7: Schematic diagram of the enolase active site residue interactions with the $(Mg^{2+})_2$–PhAH complex. Possible hydrogen bonds are shown as dashed lines; distances (Å) are the average of those for both subunits. Inhibitor bond lengths are in italics. The perspective is similar to that of Figure 6.

activity for the E168Q mutant (Brewer et al., 1993), it is probable that members of the constellation of strictly conserved residues (e.g., Glu 168, Glu 211, His 373, and Lys 396) are also important in catalysis.

Structural elements responsible for the slow-binding behavior of PhAH are enigmatic. The hydration number of metal II does not change in the early and late forms of the complex revealed by EPR (Poyner & Reed, 1992). This observation suggests that chelation of Ser 39 to metal II and flap closure are present in both early and late forms of the complex. Deletion of residues in an analogous conserved flap at the entrance to the active site of triose phosphate isomerase decreases activity by nearly 10^5 and allows escape and decomposition of the ene–diolate intermediate (Pompliano et al., 1990). The flap at the active site of enolase may have a similar function in protecting the reactive carbanion intermediate. Abell and Schloss (1991) have pointed out that such nucleophilic carbanions require protection from solvent and from electrophiles such as molecular oxygen.

ACKNOWLEDGMENT

We are grateful to Dr. Matthew Benning for advice and assistance with the molecular replacement methodology. In addition, we thank Drs. Gary Wesenberg and Hazel Holden for their assistance and advice during the progress of the refinement.

NOTE ADDED IN PROOF

While this manuscript was in press, another paper appeared on the structure of the PhAH complex of yeast enolase [Zhang, E., Hatada, M., Brewer, J. M., & Lebioda, L. (1994) *Biochemistry 33*, 6295–6300]. The structural model described in the earlier paper differs in several important respects from

the structure reported here for the cocrystallized complex at low salt in the presence of PEG. In sharp contrast to the present structure, the structure of the complex obtained by soaking inhibitor into crystals in the background of 3 M $(NH_4)_2SO_4$ provided "...no obvious explanation why PhAH binding to enolase is so much stronger than the binding of the substrates."

REFERENCES

Abell, L. M., & Schloss, J. V. (1991) *Biochemistry 30*, 7883–7887.

Anderson, V. E., & Cleland, W. W. (1990) *Biochemistry 29*, 10498–10503.

Anderson, V. E., Weiss, P. M., & Cleland, W. W. (1984) *Biochemistry 23*, 2779–2786.

Bernstein, F. C., Koetzle, T. E., Williams, G. J. B., Meyer, E. F., Jr., Brice, M. D., Rogers, J. R., Kennard, O., Shimanouchi, T., & Tasumi, M. (1977) *J. Mol. Biol. 112*, 535–542.

Bowen, S. M., Duesler, E. N., Paine, R. T., & Campana, C. F. (1982) *Inorg. Chim. Acta 59*, 53.

Brewer, J. M., Robson, R. L., Glover, C. V. C., Holland, M. J., & Lebioda, L. (1993) *Proteins: Struct., Funct., Genet. 17*, 426–434.

Bricogne, G. (1976) *Acta Crystallogr. A32*, 832–847.

Burbaum, J. J., & Knowles, J. R. (1989) *Biochemistry 28*, 9306–9317.

Castellano, E. E., Oliva, G., & Navaza, J. (1992) *J. Appl. Crystallogr. 25*, 281–284.

Chin, C. C. Q., Brewer, J. M., & Wold, F. (1981) *J. Biol. Chem. 256*, 1377–1384.

Cleland, W. W. (1992) *Biochemistry 31*, 317–319.

Dinovo, E. C., & Boyer, P. D. (1971) *J. Biol. Chem. 246*, 4586–4593.

Fox, G. C., & Holmes, K. C. (1966) *Acta Crystallogr. 20*, 886–891.

Gerlt, J. A., & Gassman, P. G. (1992) *J. Am. Chem. Soc. 114*, 5928–5934.

Gerlt, J. A., & Gassman, P. G. (1993) *Biochemistry 32*, 11943–11952.

Gerlt, J. A., Kozarich, J. W., Kenyon, G. L., & Gassman, P. G. (1991) *J. Am. Chem. Soc. 113*, 9667–9669.

Holland, M. J., Holland, J. P., Thill, G. P., & Jackson, K. A. (1981) *J. Biol. Chem. 256*, 1385–1395.

Hough, E., & Rogers, D. (1974) *Biochem. Biophys. Res. Commun. 57*, 73–77.

Jones, T. A. (1978) *J. Appl. Crystallogr. 11*, 268–276.

Kabsch, W. (1978) *Acta Crystallogr. A32*, 922–923.

Kabsch, W. (1988a) *J. Appl. Crystallogr. 21*, 67–71.

Kabsch, W. (1988b) *J. Appl. Crystallogr. 21*, 916–924.

Kraulis, P. J. (1991) *J. Appl. Crystallogr. 24*, 946–950.

Landro, J. A., Gerlt, J. A., Kozarich, J. W., Koo, C. W., Shah, V. J., Kenyon, G. L., Neidhart, D. J., Fujita, S., & Petsko, G. A. (1994) *Biochemistry 33*, 635–643.

Lebioda, L., & Brewer, J. (1984) *J. Mol. Biol. 180*, 213–215.

Lebioda, L., & Stec, B. (1989) *J. Am. Chem. Soc. 111*, 8511–8513.

Lebioda, L., & Stec, B. (1991) *Biochemistry 30*, 2817–2822.

Lebioda, L., Stec, B., & Brewer, J. M. (1989) *J. Biol. Chem. 264*, 3685–3693.

Lebioda, L., Zhang, E., Lewinski, K., & Brewer, J. M. (1993) *Proteins: Struct., Funct., Genet. 16*, 219–225.

Lee, M. E., & Nowak, T. (1992) *Biochemistry 31*, 2172–2180.

McPherson, A., Jr. (1982) *Preparation and Analysis of Protein Crystals*, p 125, Wiley, New York.

McPherson, A., Jr., & Shlichta, P. (1988) *Science 239*, 385–387.

Milburn, M. V., Tong, L., DeVos, A. M., Brünger, A., Yamaizumi, Z., Nishimura, S., & Kim, S.-H. (1990) *Science 247*, 939–945.

Navaza, J. (1987) *Acta Crystallogr. A43*, 645–653.

Navaza, J. (1990) *Acta Crystallogr. A46*, 619–620.

Neidhart, D. J., Howell, P. L., Petsko, G. A., Powers, V. M., Li, R., Kenyon, G. L., & Gerlt, J. A. (1991) *Biochemistry 30*, 9264–9273.

Petsko, G. A., Kenyon, G. L., Gerlt, J. A., Ringe, D., & Kozarich, J. W. (1993) *Trends Biochem. Sci. 18*, 372–376.

Pompliano, D. L., Peyman, A., & Knowles, J. R. (1990) *Biochemistry 29*, 3186–3194.

Poyner, R. R., & Reed, G. H. (1992) *Biochemistry 31*, 7166–7173.

Rayment, I. (1985) *Methods Enzymol. 114*, 136–140.

Read, R. J. (1986) *Acta Crystallogr. A42*, 140–149.

Richard, J. P. (1990) in *The Chemistry of Enols* (Rappoport, Z., Ed.) pp 651–689, Wiley, New York.

Russell, G. A., Dunbar, B., & Fothergill-Gilmore, L. A. (1986) *Biochem. J. 236*, 115–126.

Scopes, R. K. (1971) *Biochem. J. 122*, 89–92.

Stec, B., & Ledioda, L. (1990) *J. Mol. Biol. 211*, 235–248.

Still, C. (1989) *Macromodel Version 2.5*, Department of Chemistry, Columbia University, New York.

Stubbe, J., & Abeles, R. H. (1980) *Biochemistry 19*, 5505–5512.

Thaller, C., Eichelle, G., Weaver, L. H., Wilson, E., Karlsson, R., & Jansonius, J. N. (1985) *Methods Enzymol. 114*, 132–135.

Tronrud, D. E., Ten Eyck, L. F., & Matthews, B. W. (1987) *Acta Crystallogr. A43*, 489–501.

Weiss, P. M., Boerner, R. J., & Cleland, W. W. (1987) *J. Am. Chem. Soc. 109*, 7201–7202.

Westhead, E. W. (1966) *Methods Enzymol. 9*, 670–676.

Zalkin, A., Forrester, J. D., & Templeton, D. H. (1966) *J. Am. Chem. Soc. 88*, 1810–1814.

Zanotti, G., Monaco, H. L., & Foote, J. (1984) *J. Am. Chem. Soc. 106*, 7900.